Journal of Experimental Marine Biology and Ecology 521 (2019) 151208

Contents lists available at ScienceDirect

Journal of Experimental Marine Biology and Ecology

journal homepage: www.elsevier.com/locate/jembe

Photosynthesis and light-dependent proton pumps increase boundary layer pH in tropical macroalgae: A proposed mechanism to sustain calcification under ocean acidification

C. McNicholl[a], M.S. Koch[a,*], L.C. Hofmann[b]

[a] Biological Sciences Department, Florida Atlantic University, 777 Glades Road, Boca Raton, FL, USA
[b] Alfred Wegener Institute Helmholtz Center for Polar and Marine Research, Am Handelshafen 12, 27570 Bremerhaven, Germany

ARTICLE INFO

Keywords:
Diffusive boundary layer
Photosynthesis
Tropical
Inhibitor

ABSTRACT

Ocean acidification (OA) projections predict ocean pH to decline between 0.2 and 0.4 by 2100 with potential negative consequences for marine calcifiers without acclimation or adaption strategies to accomodate greater [H^+] in seawater. Biotic control of calcified reef macroalgae thalli surface diffusive boundary layer (DBL) chemistry may overcome low pH in seawater as one strategy to accommodate OA conditions. To investigate this strategy, we examined surface DBL O_2 and pH dynamics in five calcifying macroalgae (*Halimeda*, *Udotea*, *Jania*, *Neogoniolithon*, crustose coralline algae [CCA]) from the Florida Reef Tract under ambient (8.1) and low (7.65) pH using microsensors (100 μm) at the thalli surface in a flow-through flume. The role of photosynthesis and photosystem II (PSII)-independent proton pumps in controlling DBL pH were examined. Four of the five macroalgae exhibited a strong positive linear relationship between O_2 production and increasing pH in the first 15–30 s of irradiance. Once a quasi-steady-state O_2 concentration was reached (300 s), all species had DBL pH that were higher (0.02–0.32) than bulk seawater. The DBL pH increase was greatest at low pH and dependent on PSII. Some evidence was found for a light-dependent, but PSII-independent, proton pump. High DBL Δ pH upon illumination was likely in response to carbon concentrating mechanisms (CCMs) for photosynthesis. CCMs may be a HCO_3^-–H^+ symport, OH^- antiport or other DIC transport system, accompanied by proton efflux. HCO_3^- dehydration by external carbonic anhydrase (CA_{ext}) also produces OH^- that can neutralize H^+ in the DBL. CO_2 or HCO_3^- uptake for photosynthesis may also engage H^+/OH^- fluxes as part of intracellular acid-base regulation changing DBL pH. A higher Δ pH within the DBL at low pH could be accounted for by greater CO_2 diffusion and/or lower efficiencies in exporting cellular H^+ across a lower concentration gradient, and/or a more efficient removal of H^+ by CA_{ext}-driven dehydration of HCO_3^-. In the dark, Δ pH was less than in the light as these dynamics were primarily due to photosynthesis. We present a conceptual model of inorganic carbon uptake and ion transport pathways, as well as other processes associated with photosynthesis that drive DBL Δ pH and sustain tropical macroalgal calcification in the light under OA. In the dark, unless PSII-independent proton pumps are present, which do not appear to be ubiquitous amongst species, acidification processes likely dominate, resulting in $CaCO_3$ net dissolution, particularly under OA conditions.

1. Introduction

Ocean acidification (OA) projections (RCP2.6 and RCP8.5 AR5; IPCC et al., 2013), predict surface ocean pH to decline between 0.2 and 0.4 by 2100 (Gehlen et al., 2014; Hartin et al., 2016; IPCC, 2013). This results from ocean sequestration of ~30% of anthropogenically released CO_2 (Sabine et al., 2004) which is predicted to triple under RCP8.5 scenario to ~28 Pg C yr^{-1} by 2100 (Riahi et al., 2011). A 0.1 decrease in pH already observed in the oceans since the industrial revolution (Caldeira and Wickett, 2003) equates to a 30% increase in hydrogen ion [H^+] concentration. Ocean dissolved inorganic carbon (DIC) chemistry is influenced by changes in pH due to its regulatory effect on the carbonate equilibria. In response to a pH decrease of 0.4, the carbonate equilibria under OA leads to a ~200% increase in CO_2 and a ~25% increase in bicarbonate (HCO_3^-), while lowering carbonate (CO_3^{2-}) by ~50–60% (Fabry et al., 2008; Koch et al., 2013). The decline in CO_3^{2-} lowers the saturation state (Ω) of carbonate minerals of calcite and aragonite (~60%). The high concentration of Ca^{2+} in

* Corresponding author.
E-mail addresses: cmcnicholl2015@my.fau.edu (C. McNicholl), mkoch@fau.edu (M.S. Koch), laurie.c.hofmann@awi.de (L.C. Hofmann).

https://doi.org/10.1016/j.jembe.2019.151208
Received 19 April 2019; Received in revised form 19 July 2019; Accepted 12 August 2019

seawater (~10,000 μmol kg^{-1}) is considered non-limiting for calcification, thus calcium carbonate production is chemically controlled by the concentration (100–200 μmol kg^{-1}) of CO_3^{2-} (Millero, 2007; Millero et al., 2006). The reduction in CO_3^{2-} under OA is a major concern because of the potential negative consequences for calcification in marine organisms (Doney et al., 2012; Doney et al., 2009; Fabry et al., 2008; Gattuso et al., 2015; Kroeker et al., 2010; Orr et al., 2005; Sabine et al., 2004). Calcification rates have been shown to be correlated to seawater Ω_{CaCO3} and studies indicate higher calcification rates under elevated [CO_3^{2-}] (Anthony et al., 2008; Gao et al., 1993; Gattuso et al., 1999; Hoegh-Guldberg et al., 2007; Langdon et al., 2000).

While the saturation state of $CaCO_3$, [CO_3^{2-}], and [Ca^{2+}] are recognized as important for calcifiers (Comeau et al., 2012; Waldbusser et al., 2016), some studies show no relationship between calcification rates and Ω_{CaCO3} in the bulk seawater and inconsistent calcification responses by a diversity of marine organisms to lower Ω_{CaCO3} (Comeau et al., 2018; Comeau et al., 2016; Dutra et al., 2015; Hendriks et al., 2010; McDonald et al., 2009; Peach et al., 2017b; Rodolfo-Metalpa et al., 2011; Shamberger et al., 2014). These results led Jokiel (Jokiel, 2013, 2011) and others (Bach, 2015; Cyronak et al., 2015) to re-evaluate the importance of Ω_{CaCO3} and put forth an alternative hypothesis. They suggest that limitations to calcification are a consequence of a buildup of [H^+] at the site of calcification due to an inability to expel protons from the calcifying space into the bulk seawater under OA conditions. However, this theory is based primary on corals where mineralization is below an epithelial layer separating the calcification site from seawater, while marine macroalgae calcify in their cell walls and extracellularly in close proximity to bulk seawater. In macroalgae, the diffusive boundary layer (DBL) microchemistry, driven by cellular metabolic processes, membrane transport systems and/or thalli morphologies control the calcification site exposure to bulk seawater chemistry.

Therefore, the question for macroalgae is can they control their DBL chemistry through proton pumps and employ mechanisms to take up CO_2 and HCO_3^- that raise DBL pH and maintain calcification under OA. Relatively new applications of the boron isotope provide evidence that marine calcifiers, including corals and calcifying algae, have the capacity to maintain a high pH in their calcifying fluid (pH_{cf}) even under OA conditions (pH 7.64) where [CO_3^{2-}] and Ω_{CaCO3} of the bulk seawater are low (Comeau et al., 2018; Cornwall et al., 2017a; Donald et al., 2017; McCulloch et al., 2012). Understanding these mechanisms are particularly critical in calcifying autotrophs that require HCO_3^- and/or CO_2 for photosynthesis (Hurd et al., 2011; Koch et al., 2013), a major driver of high calcification rates (De Beer and Larkum, 2001), and in some species initiates calcification (Wizemann et al., 2014). For marine calcifying macroalgae, the increase in HCO_3^- and CO_2 under OA promote DIC availability for photosynthesis (Cornwall et al., 2017b; Koch et al., 2013; Zweng et al., 2018). Greater [DIC] may result in higher rates of calcification or compensate for OA effects, as photosynthesis and calcification may be in competition for DIC or control the DIC/H^+ ratios affecting calcification. Further, the majority of marine macroautotrophs are restricted to energetics from photosynthesis, while corals and other heterotrophs can acquire energy to maintain a high pH_{cf} through feeding (McCulloch et al., 2012).

Several recent studies examining the thallus boundary conditions of marine macroalgal calcifiers indicate a high degree of biotic control to elevate pH in the light at the thalli surface (Cornwall et al., 2014, 2013; Hofmann et al., 2018, 2016; Hurd et al., 2011) and in their calcifying fluids (Comeau et al., 2018; Cornwall et al., 2017a; Donald et al., 2017). As pH increases at the thalli surface across species and calcification location, a general model may emerge on the role of biotic pH control on calcification with closer examination of a diversity of calcifying macroalgae. In the present study, five tropical reef macroalgae were examined for their ability to regulate thalli surface DBL pH when bulk seawater pH was reduced from ambient conditions (8.1) to those projected for the year 2100. Microsensors were used to establish pH and O_2 dynamics to discern potential mechanisms controlling DBL microchemistry under OA conditions and how these DIC and ion fluxes may subsequently influence calcification. The DBL pH dependence on light, photosynthesis, and light-dependent photosystem II-independent proton pumps were also examined for each species. We present a general conceptual model to formulate our hypothesis of how DIC pathways and biotic control of pH could shift under OA and subsequently affect calcification.

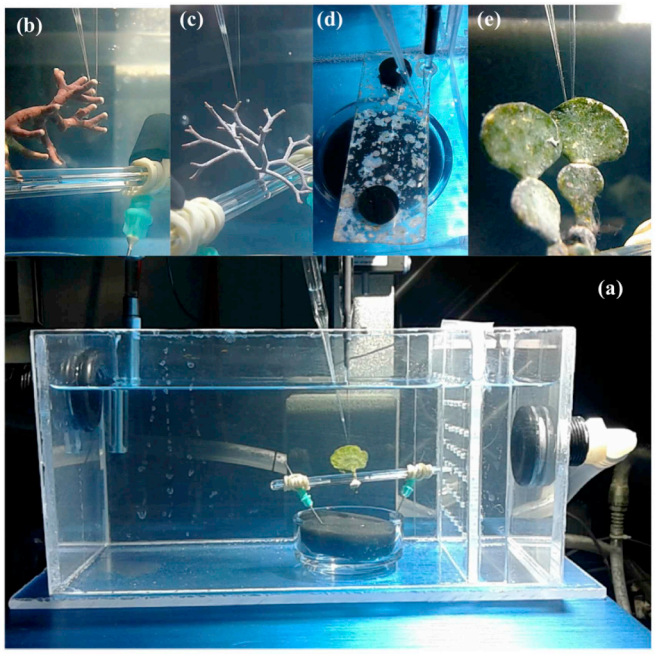

Fig. 1. Images of the (a) experimental flow-through flume system illustrating the setup of macroalgae and pH (black) and O_2 (clear) microsensors at the thalli surface of *Udotea*. The other species (b = *Neogoniolithon*, c = *Jania*, d = CCA, e = *Halimeda*) are also depicted with microsensor tips positioned at the thalli surface.

2. Methods

2.1. Algal collection

Five dominant calcified Florida Reef Tract macroalgae (Fig. 1) were collected from a patch reef (~4 m depth) inshore of Looe Key Reef and offshore of Big Pine Key, FL (24° 37.233′ N, 81° 22.247′ W; Oct 2017 – Jan 2018); hereafter referred to by genus names. The five tropical reef calcifiers in this study include: three high-Mg calcite rhodophytes (*Neogoniolithon strictum* and *Jania adhaerens* [branching], and crustose coralline algae (CCA) [prostrate]) and two aragonite filamentous chlorophytes (*Halimeda scabra* [segmented, branching plates] and *Udotea luna* [fan shaped]). CCA was collected following establishment onto settlement plates (2 × 6 cm) over a 4-month period. All species and settlement plates were transported back to the Florida Atlantic University (FAU) lab in an aerated cooler and experiments run within two weeks. During collections, irradiance was determined using an underwater 4π spherical quantum sensor (LI-COR). Temperature, salinity and O_2 of the overlying water were measured using a multisensor probe (600 XLM, YSI Inc.). Surface water pH was also measured from discrete samples (Orion A211, 8302BNUMD) following calibration with NBS standards pH 7.00 and 10.00 and corrected with a standard TRIS buffer (Dickson Lab, Scripps Institute of Oceanography). Seawater samples (150 mL) from the collection site were stored cooled (4 °C) in the dark and total alkalinity (TA) determined by titration within 48 h.

Algae were held in 9 L aquaria with seawater (35 psu) collected from FAU's marine lab (Atlantic Ocean, Boca Raton, FL) in a water-bath

maintained at 28 °C and illuminated (~300 μmol photons $m^{-2} s^{-1}$) under a 12 h day/night cycle. Aquaria seawater was replenished (75%) every other day to maintain salinity and provide nutrients with pH and TA similar to collection site (8.09 and 2298 μmol kg^{-1} sw, respectively); aquaria were continuously aerated.

2.2. Microsensors and experimental setup

Microsensor measurements were conducted in a flow-through flume system (Fig. 1a) using filtered (0.45 μm) seawater from the FAU marine lab maintained at 28 °C. Flume seawater pH_{NBS} was continuously measured (1 min) in the flume (Orion A211, 8302BNUMD) after calibration and corrected with a TRIS buffer (Dickson Lab, Scripps Institute of Oceanography). The O_2 was measured using an optical sensor (Orion A329) at the beginning and end of each microsensor experiment. During each run, TA was determined on flume seawater and used to calculate carbonate speciation with CO2SYS (Pierrot et al., 2006). Carbonate chemistry parameters were calculated using the pH treatments and average Florida Reef tract temperature (28 °C) and salinity (35 psu) used for microsensor runs. The pCO_2 treatment was 1200 μatm for low pH (7.66 ± 0.02) and 360 ± 28 μatm for ambient pH (8.12 ± 0.03) controls (Table S1). The calcium carbonate saturation state ($\Omega_{Ca/Arag}$) of aragonite and calcite were 2–3 times higher in the ambient controls (6.0/3.8) relative to low (2.5/1.6) pH treatments (Table S1). The Δ pH during the runs in the bulk seawater from the initial to end of experiments was 0.01 to 0.03.

Within the flume system, macroalgae were secured approximately 10 cm from the chamber bottom in the center of the flume to receive laminar flow (Fig. 1a–e). Water flow was provided by a submersible 300 L hr^{-1} pump in the sump tank. Seawater was pumped from the sump to the flume where seawater passed through a perforated barrier in order to create laminar flow. Laminar flow and velocity were previously determined by injecting dye into the sump tank and recording flow in the flume. The flume was illuminated by a full-spectrum LED light (Kessil, A360W *E*-Series Tuna Sun) set at 500 μmol photons $m^{-2} s^{-1}$ during light runs. The O_2 and pH microsensors were positioned within 200 μm of each other on the thalli surface using a manual dual-head micromanipulator arm (MM33–2, Unisense) and measurements set to record simultaneously every second. Thalli surface O_2 and pH dynamics were determined using miniaturized amperometric sensors detecting oxidation-reduction signals (pA range) with rapid response times (0.3 s) and recorded with a highly sensitive picoammeter (Unisense UnderWater Meter System, Denmark). The microsensors (100 μm) are connected to a 4-channel underwater recorder equipped with amplifiers (ISA) that provide a high-quality signal with low background interference. Prior to measurements, the sensors are polarized and calibrated. The O_2 microsensor (OX-100, Unisense Inc.) was calibrated using aerated seawater at 100% saturation and an anoxia solution used for 0% saturation (0.1 M sodium ascorbate and NaOH; ~2 g sodium ascorbate in 100 mL of 0.1 M NaOH). The pH microsensor (pH -100, Unisense Inc.) was calibrated using NBS buffers (7.00 and 10.00) and corrected using a TRIS buffer (Dickson Lab, Scripps Institute of Oceanography).

2.3. pH and O_2 dynamic experiments

After samples were secured in the flume and microsensors moved into position, light:dark cycle runs proceeded. There was an initial 10-min dark pretreatment period followed by 3 continuous light:dark cycles run at 5 min intervals. The first was conducted at a pH of ~8.1 (ambient). The flume seawater or bulk water pH was then lowered to ~7.65 (low pH) by the addition of acidified seawater produced by bubbling with pure CO_2 (Riebesell and Gattuso, 2011) and added in 20 ml aliquots to the water bath in line with the flume system. Once bulk seawater pH and thalli microsensor pH stabilized, the algae was again pretreated for 10 min in the dark, followed by another light:dark cycle. At the end of the low pH light:dark cycle, the bulk seawater pH was adjusted to pH 8.1 by adding 0.05 M NaOH in 2 ml aliquots to the water bath and inhibitor experiments conducted. Test runs showed no difference in pH and O_2 surface dynamics after the addition of NaOH to re-establish ambient pH conditions, and adjustments were only performed before the inhibitor experiment.

To determine the role of photosynthesis in thallus surface pH dynamics, a photosystem II inhibitor, herbicide 3-(3,4-Dichlorophenyl)-1,1-dimethylurea (DCMU), was amended to the flume system. The concentration to be used for each run was established by the minimum level needed to inhibit O_2 production at the thalli surface of the species examined (~2–4 μM DCMU). Although DCMU has been shown to elevate respiration in some macroalgae, no change in [O_2] was found with DCMU for any species or run (Table S2). Diminished O_2 concentrations at the thalli surface and no O_2 change under irradiance was used to confirm photosynthesis inhibition before light:dark cycles commenced. The light:dark cycle runs were conducted at pH 8.1 and 7.65 as described above.

3. Statistical analysis

To compare amongst treatments and define O_2 and pH dynamics, *t*-tests and regression analyses were performed (SigmaPlot 13.0, Systat Software Inc.). A t-test was used to examine O_2 and pH changes at the thalli surface in response to light (light-dark) and pH (ambient-low) changes. For these comparisons, the average of the first and last 10 s of the dynamic runs ($n = 3$) were calculated and the differences used in the analysis. The same approach was used for the runs with the photosynthetic inhibitor (DCMU). Thalli surface pH was also compared to the bulk seawater pH in the light and dark, as well as in the ambient and low pH treatments. A Mann-Whitney U non-parametric test was used if data were non-normal or variances were not homogeneous. Linear regression analysis was used to establish the relationship (slope, R^2) between photosynthesis (O_2 production) and pH change using the initial 30 s of the light run. The dynamics in the light and dark across the entire 300 s dynamic run were described using linear and non-linear regression analysis.

4. Results

4.1. Microsensor runs

Three independent microsensor runs using different individuals produced a range of thalli surface O_2 concentrations after 300 s for each species ranging from 73 to 852 μM of O_2 (Table 1). However, the replicates within each microsensor run were highly repeatable with low variance across three sequential light-dark cycles and pH treatments (Fig. 2). Thus, pH and light-dark comparisons of O_2 and pH dynamics were examined within each run (Tables 1–3), and details of the dynamics are presented in graphs for light-dark incubations in microsensor run one (Figs. 2–4) with additional runs presented in the supplement (Fig. S1, S2).

4.2. Dark-light O_2 dynamics

The change in O_2 from dark to light in ambient, compared to low pH, was not significant for most of the species across all three microsensor runs (Fig. 2; Table 1) with the exception of CCA and *Halimeda* in runs one and two. During these runs, the change in O_2 in response to light was always greatest at low pH. Although these results indicate a potential increase in photosynthesis with greater CO_2 availability at low pH, the percent increase was only 21 and 23% for CCA and *Halimeda*, respectively. The consistency of O_2 dynamic changes from light to dark incubations is clearly seen in the replicate incubations in run one where the O_2 scale was equivalent for both ambient and low pH runs (Fig. 2) and in runs two and three (Table 1). In contrast to relatively high [O_2]

Table 1
Changes in O_2 concentrations from dark to light conditions at the thalli surface (Neo = *Neogoniolithon*, Jan = *Jania*, CCA, Hal = *Halimeda*, Udot = *Udotea*) under ambient (8.1) and low (7.65) pH with and without the photosynthetic inhibitor DCMU. Replicate microsensor experiments are shown with sequential 300 s dark/light cycles (AVG ± SD; n = 3). Data are averages of the last 10 s in the light/dark for each run. Runs 1–3 without DCMU and 1–2 with DCMU. Means with asterisk represent significant differences between ambient and low pH ($P < .05$).

	△ Oxygen (μM)					
	Microsensor Run 1		Microsensor Run 2		Microsensor Run 3	
(a)	Ambient	Low	Ambient	Low	Ambient	Low
Neo	442 ± 9	421 ± 21	852 ± 63	737 ± 51	256 ± 44	271 ± 26
Jan	328 ± 49	304 ± 48	131 ± 11	170 ± 6	123 ± 9	148 ± 2
CCA	236 ± 12*	265 ± 8*	137 ± 9*	173 ± 7*	213 ± 20	230 ± 32
Hal	559 ± 26*	608 ± 14*	139 ± 10*	190 ± 4*	242 ± 11	236 ± 14
Udot	83 ± 4	71 ± 7	73 ± 3	78 ± 4	101 ± 12	104 ± 6
(b)	△ Oxygen (μM) (+ DCMU)					
Neo	6 ± 2	9 ± 0	9 ± 4	17 ± 5	nd	
Jan	3 ± 4	−3 ± 6	7 ± 3	5 ± 7	nd	
CCA	21 ± 3	21 ± 2	10 ± 3	5 ± 4	nd	
Hal	23 ± 2	22 ± 2	−1 ± 3	2 ± 4	nd	
Udot	−1 ± 4	1 ± 2	5 ± 6	−2 ± 6	nd	

in the light, DCMU [O_2] were 1 to 2 orders-of-magnitude lower (Table 1). Further evidence of DCMU's efficiency in arresting photosynthesis is shown by a negative [O_2] difference between the thalli surface and bulk seawater [O_2] (surface-bulk) in the light for all species in the presence of DCMU (Table S2).

4.3. Dark-light pH dynamics

The initial (15–30 s) light-induced increase in pH at the thalli surface was highly correlated with O_2 production (R^2 0.86–0.98) for all species (Fig. 3a–d) with the exception of CCA (Fig. 2c). The slope of the initial pH response was relatively similar under ambient and low pH (Fig. 3a–d), but was an order of magnitude greater for *Halimeda* compared to the other species (Fig. 3c). While CCA had an immediate O_2 flux response to light, there was a lag in pH increase (Fig. 2c).

In contrast to short-term (15–30 s) pH dynamics, over the entire 300 s light incubation, Δ pH was greater under the low pH treatment (0.12) compared to ambient pH (0.09). This ~38% increase in pH was observed for almost every microsensor run (24–46% change) and for all species with the exception of *Udotea* (Table 2). A significantly higher Δ pH dark/light cycle (280–300 s) between ambient and low pH incubations was observed in two runs for *Halimeda* and one run for *Neogoniolithon* and *Jania*, although all average changes in pH for these species tended to be higher at low pH relative to ambient controls (Table 2). The greatest increase in pH during the light cycle was 0.42 and 0.31 units for *Halimeda* and *Jania*, respectively, in the low pH treatment during run one. Further, the slopes of pH change over time for the entire 300 s incubation (Table 4) were always higher in the low compared to ambient pH incubation based on the non-linear and linear models (Fig. 4, light). The pH dynamics for all species in the light followed an exponential function with the exception of CCA. CCA pH increased linearly in two distinct phases with the first peaking at 100 s, followed by a slow increase that appeared to level off in the ambient pH treatment, but continued to increase in the low pH treatment (Fig. 4c light).

The pH dynamics in the dark were similar for *Neogoniolithon*, *Jania* and *Udotea* which all followed a hyperbolic decay model with relatively similar slopes at low and ambient pH (Fig. 4a, b, e; Table 4). The non-linear models of pH decline in the dark were similar between pH treatments compared to more diverse responses in the light. *Halimeda* showed a rapid decline in pH during the dark incubation for the first 100 s, followed by an increase in pH, fitting an exponential decay function with a linear combination (Fig. 4d, Table 4). Consistent with the light dynamics, CCA had a slow 2-phase decline in pH over time, but still fit the hyperbolic decay model.

Following treatment with DCMU, Δ pH from dark to light was lowered significantly. There was also no difference in the Δ pH under ambient and low pH. Thus, the dark/light changes in pH at the thalli surface was dependent on photosynthesis for most species. The greater Δ pH under OA conditions was also linked to photosynthesis, as no significant differences in Δ pH at low pH were observed after treatment with DCMU. Only 2 species (*Neogoniolithon*, *Halimeda*) continued to exhibit pH dynamics during the dark-light cycles with DCMU, albeit the magnitude of change was significantly reduced. Both at ambient and low pH, *Neogoniolithon* had the capacity to raise pH ~0.03 to 0.04 units in the light following a 300 s dark incubation (Fig. 5). *Halimeda* showed an inverse response to *Neogoniolithon*, increasing pH ~0.03 to 0.04 units in the dark, and lowering pH at the thalli surface in the light (Fig. 5). This increase in pH during the dark incubation for *Halimeda* is consistent with the 300 s dark incubation that showed an exponential decrease in pH followed by a slower linear rise over time (Fig. 4d).

4.4. Thalli surface vs bulk seawater pH

In addition to ~33% greater Δ pH between dark-light cycles at low compared to ambient pH, we observed a 133% increase in pH at the thalli surface relative to the bulk seawater pH at low compared to ambient pH in the light. Averaging results from all five species, there was a higher pH at the thalli surfaces relative to the bulk seawater at low (average = 0.14) compared to ambient (average = 0.06) pH in the light, and significant differences detected for at least two out of three runs for each species (Table 3). Even in the dark, the pH was higher at the thalli surface relative to bulk seawater in the low pH treatments compared to ambient pH controls (Table 3). During the entire run (Fig. 2) a higher Δ pH was maintained at the thalli surface relative to the bulk seawater at low compared to ambient pH.

5. Discussion

Four out of five tropical calcifying reef macroalgae exhibited a strong linear relationship between O_2 production and increasing pH in the first 15–30 s of the runs, with two of the rhodophyte species (*Neogoniolithon* and *Jania*) and *Halimeda* exhibiting an $R^2 \geq 95$. Once a quasi-steady-state O_2 concentration was reached after 300 s in the light,

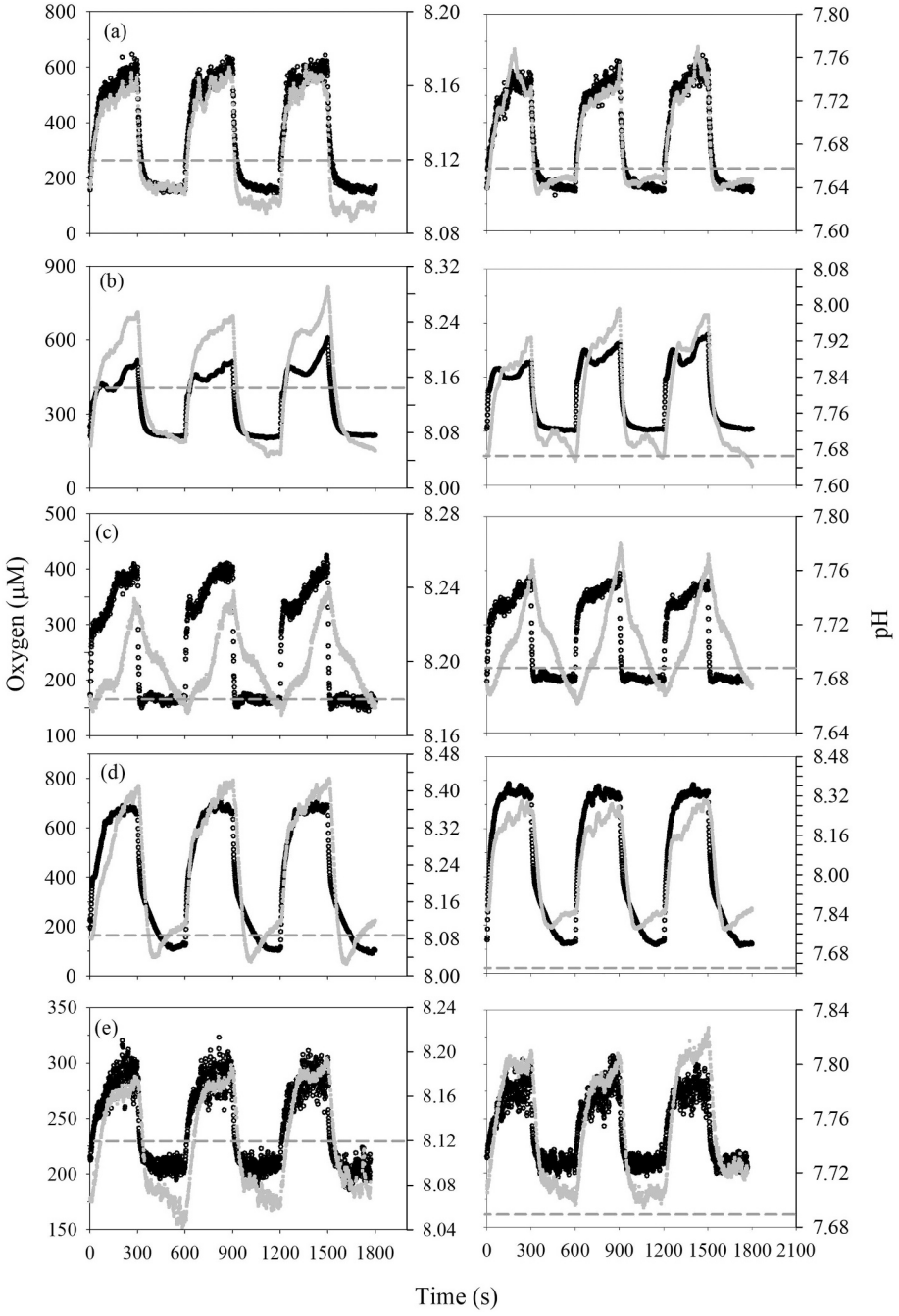

Fig. 2. Complete dark-light cycles (n = 3) showing O_2 (dark circles) and pH (grey circles) thalli surface dynamics for each species (a = *Neogoniolithon*, b = *Jania*, c = CCA, d = *Halimeda*, e = *Udotea*). Panels on left show dynamics at ambient pH, while those on the right are at low pH; note different right axis scale for pH treatments. The bulk seawater pH is also shown (grey dotted line) in each figure. Each cycle starts with lights (500 µmol photons $m^{-2} s^{-1}$) on for 300 s followed by a 300 s dark period.

pH at the thalli surfaces was always greater (0.02–0.32) than in the overlying bulk seawater for all species. This increase in pH at the thalli surface was primarily dependent on photosynthesis, as shown by no significant Δ pH between ambient and low pH treatments when PSII was inhibited with DCMU. A metabolically-driven increase in pH within the diffusive boundary layer (DBL) in the light has been observed in fleshy (Noisette and Hurd, 2018) and calcifying (Cornwall et al., 2015, 2013; De Beer and Larkum, 2001; Hofmann et al., 2018, 2016; Hurd et al., 2011) macroalgae. Encrusting coralline algae (*Sporolithon durum*) raised pH in the light 0.88 pH units from 8.0 pH after 1 h under a flow rate of 1.5 cm s^{-1} (Hurd et al., 2011), similar to the flow in our experiments (~2–3 cm s^{-1}). Cornwall et al. (2013) attributed a pH increase of ~0.35 in the light within the DBL of an erect coralline and encrusting algal consortium at flow rates < 4 cm s^{-1} to photosynthesis. Photosynthetic inhibitors (AZ, DIDS) lowered a 0.3 to 0.7 pH increase by ~30% at the surface of a crustose coralline algae (CCA) (Hofmann et al., 2016). These data, and those showing a correspondence between increasing CO_3^{2-} and pH at algal surfaces using microsensors (Chrachri et al., 2018; Hofmann et al., 2018), infer that photosynthesis drives pH and DIC microchemistry within the DBL by the exchange of CO_2 and ions (H^+, OH^-, HCO_3^-) across the plasmalemma (Borowitzka, 1981; Borowitzka and Larkum, 1987; Gao et al., 1993). HCO_3^- uptake via a H^+ symport (or OH^- antiport) or other H^+ transport mechanism (e.g., Ca^{2+}:H^+ antiport, Na^+:H^+ antiport) and/or external carbonic

Table 2
Changes in pH from dark to light conditions at the thalli surface (Neo = *Neogoniolithon*, Jan = *Jania*, CCA, Hal = *Halimeda*, Udot = *Udotea*) under ambient (8.1) and low (7.65) pH with and without the photosynthetic inhibitor DCMU. Replicate microsensor experiments are shown with sequential dark/light cycles (AVG ± SD; n = 3). Runs 1–3 without DCMU and 1–2 with DCMU. Data are averages of the last 10 s in the light/dark for each run. Means with asterisk represent significant differences between ambient and low pH ($P < 0.05$).

	△ pH					
	Microsensor Run 1		Microsensor Run 2		Microsensor Run 3	
	Ambient	Low	Ambient	Low	Ambient	Low
Neo	0.062 ± 0.004*	0.090 ± 0.007*	0.100 ± 0.002	0.118 ± 0.013	0.064 ± 0.009	0.090 ± 0.007
Jan	0.202 ± 0.023*	0.306 ± 0.037*	0.061 ± 0.011	0.071 ± 0.002	0.031 ± 0.004	0.028 ± 0.003
CCA	0.054 ± 0.005	0.082 ± 0.005	0.032 ± 0.004	0.032 ± 0.007	0.031 ± 0.003	0.042 ± 0.011
Hal	0.295 ± 0.006*	0.418 ± 0.014*	0.029 ± 0.005*	0.054 ± 0.005*	0.072 ± 0.009	0.093 ± 0.011
Udot	0.119 ± 0.007*	0.100 ± 0.004	0.029 ± 0.017	0.018 ± 0.004	0.055 ± 0.029	0.027 ± 0.011
	△ pH (+DCMU)					
Neo	0.014 ± 0.001	0.015 ± 0.001	0.006 ± 0.009	0.012 ± 0.013	nd	
Jan	−0.012 ± 0.007	0.015 ± 0.012	−0.013 ± 0.005	−0.012 ± 0.006	nd	
CCA	−0.013 ± 0.001	−0.020 ± 0.004	0.013 ± 0.012	0.000 ± 0.000	nd	
Hal	−0.022 ± 0.039	−0.032 ± 0.025	−0.035 ± 0.007	−0.030 ± 0.008	nd	
Udot	−0.013 ± 0.009	−0.020 ± 0.002	−0.001 ± 0.003	−0.001 ± 0.004	nd	

anhydrase enzyme (CA_{ext})-mediated dehydration of HCO_3^- to CO_2 and OH^- would raise the pH at the thallus surface. HCO_3^- dehydrogenation by CA_{ext} to CO_2, followed by diffusive flux into the cell for photosynthesis, was predicted by Chrachri et al. (2018) to drive a rapid pH change in the DBL of large diatoms. Active HCO_3^- uptake and CO_2 diffusion mediated by CA_{ext} may be not be exclusive. A H^+ efflux across the plasmalemma, catalyzed by a H^+-ATPase in support of a HCO_3^-/H^+ symport, would create microzones of low pH that would enhance external dehydration of HCO_3^-. While suspected to occur, these low pH microzones at the thalli surface have not been identified (Raven and Hurd, 2012). Although the CA_{ext} enzyme speeds up the equilibria reactions between HCO_3^- and CO_2, an initial mechanism is required to initiate a shift in the carbonate equilibria. Support for additional HCO_3^- transport mechanisms have been evidenced by incomplete reduction in photosynthetic rates (O_2 flux) using CA_{ext} inhibitors in both macroalgae (Hofmann et al., 2016) and phytoplankton (Chrachri et al., 2018). In addition to direct effects, intracellular acid-base regulation in response to photosynthesis can generate H^+/OH^- fluxes across the plasmalemma shifting DBL pH. Regardless of the DIC-uptake or ion transport mechanism, photosynthesis promotes Δ pH which has been attributed to maximum rates of calcification in macroalgae and corals (De Beer and Larkum, 2001; Gattuso et al., 1999; Martin et al., 2013). Thus, an

Table 3
Differences between bulk seawater and thalli surface (Neo = *Neogoniolithon*, Jan = *Jania*, CCA, Hal = *Halimeda*, Udot = *Udotea*) pH (surface – bulk) in the light and dark under ambient (8.1) and low (7.65) pH conditions and with and without the photosynthetic inhibitor DCMU in the light. Replicate microsensor experiments are shown with replicate light measurements (AVG ± SD; n = 3). Data are averages of the last 10 s in the light/dark for each run. Runs 1–3 without DCMU and 1–2 with DCMU. Means with asterisk represent significant differences between ambient and low pH ($P < 0.05$).

I) Light	△ pH					
	Microsensor Run 1		Microsensor Run 2		Microsensor Run 3	
	Ambient	Low	Ambient	Low	Ambient	Low
Neo	0.040 ± 0.004*	0.077 ± 0.007*	0.030 ± 0.017	0.050 ± 0.022	0.032 ± 0.010*	0.095 ± 0.005*
Jan	0.111 ± 0.020*	0.294 ± 0.035*	0.060 ± 0.005*	0.092 ± 0.007*	0.017 ± 0.003	0.071 ± 0.012
CCA	0.052 ± 0.004*	0.073 ± 0.006*	0.040 ± 0.014	0.040 ± 0.003	0.041 ± 0.002*	0.092 ± 0.016*
Hal	0.320 ± 0.008*	0.650 ± 0.021*	0.037 ± 0.005	0.096 ± 0.025	0.018 ± 0.004*	0.073 ± 0.020*
Udot	0.062 ± 0.008*	0.120 ± 0.009*	0.030 ± 0.008	0.015 ± 0.005	0.016 ± 0.003*	0.060 ± 0.004*
	△ pH (+DCMU)					
Neo	−0.033 ± 0.006	−0.029 ± 0.003	−0.063 ± 0.010	−0.090 ± 0.010	nd	
Jan	−0.061 ± 0.008	−0.053 ± 0.020	−0.066 ± 0.002	−0.010 ± 0.018	nd	
CCA	−0.003 ± 0.000	−0.003 ± 0.012	−0.030 ± 0.011	−0.014 ± 0.002	nd	
Hal	−0.133 ± 0.047	−0.060 ± 0.030	−0.044 ± 0.008	0.011 ± 0.018	nd	
Udot	−0.063 ± 0.002	−0.005 ± 0.011	0.049 ± 0.004	−0.032 ± 0.007	nd	
II) Dark	△ pH					
Neo	−0.022 ± 0.004*	−0.013 ± 0.001*	−0.093 ± 0.033	−0.068 ± 0.011	−0.032 ± 0.001*	0.005 ± 0.002*
Jan	−0.092 ± 0.009*	−0.012 ± 0.009*	−0.054 ± 0.009*	0.021 ± 0.008*	−0.013 ± 0.002*	0.042 ± 0.009*
CCA	−0.003 ± 0.001	−0.018 ± 0.003	0.007 ± 0.011	0.008 ± 0.007	0.009 ± 0.003	0.050 ± 0.009
Hal	0.025 ± 0.002*	0.233 ± 0.007*	0.009 ± 0.000	0.042 ± 0.022	−0.055 ± 0.006*	−0.021 ± 0.012*
Udot	−0.057 ± 0.015*	0.020 ± 0.012*	0.001 ± 0.011	−0.003 ± 0.001	−0.037 ± 0.025*	0.033 ± 0.010*

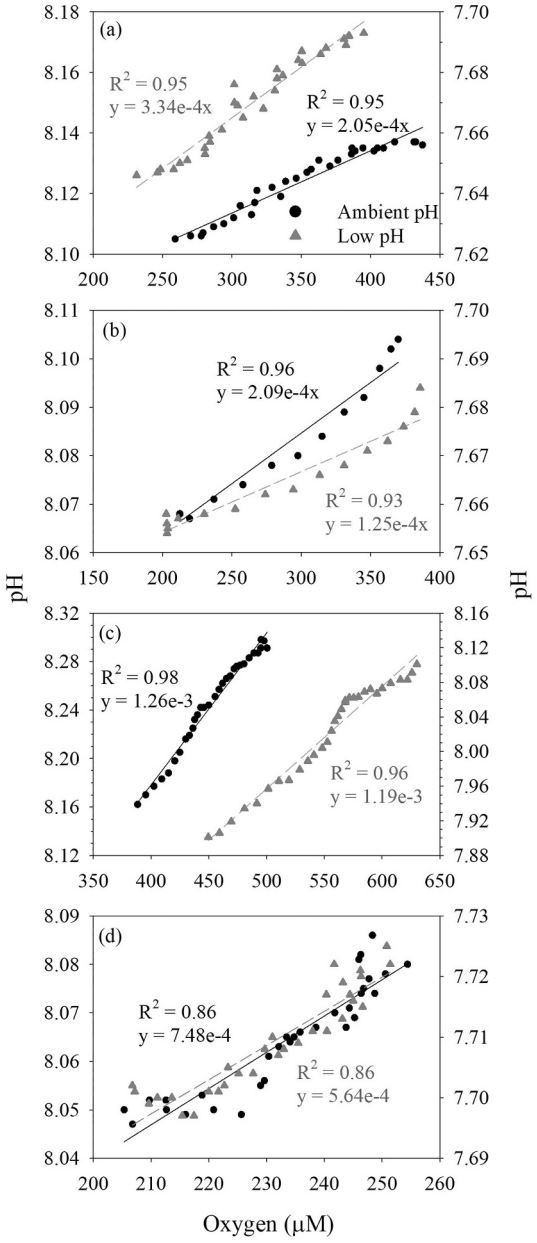

Fig. 3. Linear pH change in response to photosynthesis (O_2 flux) during the first 15–30 s in the light following 300 s in the dark for a = *Neogoniolithon*, b = *Jania*, c = *Halimeda*, d = *Udotea*. Each point is the average of the 3 light cycles at that time step (Fig. 2). Slopes and R^2 are shown on the graph for incubations at ambient (dark circles, solid line) and low (grey triangles, dashed line) pH.

important question is whether or not photosynthesis and increase of the DBL pH with photosynthesis will be compromised at low pH under OA.

Based on our microsensor data, O_2 flux at the thalli surface upon irradiance was relatively similar at 7.65 and 8.1 pH for all species, indicating that photosynthesis was not constrained by low pH. In fact, the O_2 concentration at the thalli surface in the light was significantly higher on average for two species (*Halimeda* and CCA) in the low, compared to ambient pH treatment. While increased photosynthesis in response to elevated DIC and CO_2 is not ubiquitous across macroalgal species (Cornwall et al., 2012; reviewed in Koch et al., 2013), the tropical calcifiers examined herein, with the exception of CCA and *Neogoniolithon*, increased P_{gmax} at pH 7.5 relative to pH 8.5 at high saturating irradiances (Zweng et al., 2018). Thus, they are likely facultative HCO_3^- users, also supported by their organic $\delta^{13}C$ isotope ratios (−14 to −20; Zweng et al., 2018) that suggest they acquire both HCO_3^- and CO_2 (Johnston et al., 1992; Maberly et al., 1992).

Even though relatively similar Δ pH dynamics were observed at ambient and low pH, thalli surface pH was always greater than bulk seawater in the light for all species under OA conditions. These results may partially be explained by a lower buffering capacity in the low pH seawater (Ravelle Factor; RF). However, pH in the DBL was always higher at low pH relative to bulk seawater, the increased Δ pH was always positive, and the pH change was faster than predicted based on chemical equilibria (CO2SYS RF change with pH). Enhanced Δ pH under OA conditions was arrested with DCMU, lending further support for a biotically-controlled process, or one linked to PSII in the light. A similar response was found in a tropical CCA where surface pH was raised 0.6 units at pH 7.8, while only 0.25 at pH 8.1 from dark to light (Hofmann et al., 2016). Recent studies using boron isotopes have also shown that pH_{cf} is increased at low (~0.5 to 1.0 pH units at 7.64 pH) compared to ambient pH (~0.2 to 0.8 pH units at 8.08) in coralline algae (Cornwall et al., 2017a). Also using boron isotopic proxies, the rhodolith *Neogoniolithon* sp. was found to increase pH_{cf} 1.26 pH units at pH 7.64, an almost 2-fold greater Δ pH (0.85) than under ambient (8.19) pH (Donald et al., 2017). An increase in pH within the DBL relative to the bulk seawater could be a consequence of greater CO_2 diffusion and/or lower export of cellular H^+ as the plasma membrane proton motive force reverses under OA (Taylor et al., 2012). Alternatively, the carbonate equilibria shift towards CO_2 under lower pH may increase CA_{ext}-facilitated CO_2 uptake resulting in more H^+ being neutralized by OH^- in the DBL, or enhanced cellular acid-base regulation increasing DBL pH.

Biotic control of Δ pH in the DBL without PSII was only consistently observed for two species, *Halimeda* and *Neogoniolithon*, although *Jania* depicted similar, but inconsistent, dynamics to *Neogoniolithon*. In the presence of DCMU, light/dark DBL Δ pH was only ~0.05 units and in opposite directions. The divergent species-specific patterns of H^+ efflux within the DBL with respect to the light can be reconciled by considering their respective morphologies and calcification sites. *Halimeda* is made up of tightly joined filaments that form a semi-enclosed intercellular space (ICS) interior to appressed swollen end filaments (utricles). At the surface of these appressed cells, small (~3–500 µm; Borowitzka and Larkum, 1987; Peach et al., 2017a) ion diffusion channels form (De Beer and Larkum, 2001) that may have a light-dependent, but PSII independent, proton pump. Lower pH in the DBL from H^+ efflux was observed in the light with DCMU, but was presumably masked by high Δ pH when PSII was operational. One explanation is that in the light, Ω_{CaCO3} is raised by pumping H^+ out of the utricular space, lowering surface pH outside the utricles. A similar inverse pH dynamic was observed by De Beer and Larkum (2001) with microsensors at the surface of *Halimeda discoidea*. In our dynamic observations, the *Halimeda* H^+ pump, potentially a proton ATPase or sodium-proton exchange driven by a sodium ATPase (Gimmler, 2000) was inhibited or reversed in the dark. This reverse dynamic was modeled in the non-DCMU treatments in the dark by an exponential decay function with a linear combination. In *Halimeda*, net calcification in the light without photosystem II was 30% of controls, and this species showed little to no net calcification in the dark (McNicholl and Koch, unpublished data). Thus, photosynthesis is a major driver for calcification (~70%), but a light dependent, potentially a proton ATPase pump, independent of PSII electron transport, may also be important.

In contrast to *Halimeda*, *Neogoniolithon* DBL pH increased in the light with DCMU, indicating a proton pump independent of PSII that could potentially enhance calcification within the cell wall. Support for a non-PSII light-driven calcification mechanism in this species is provided by greater net calcification rates in the light with DCMU compared to the dark (McNicholl and Koch, unpublished data). The subsequent declining pH may be associated with H^+ efflux from calcification. The rhodophytes as a group are known to biotically control calcification and dissolution processes that have been linked to the formation of distal

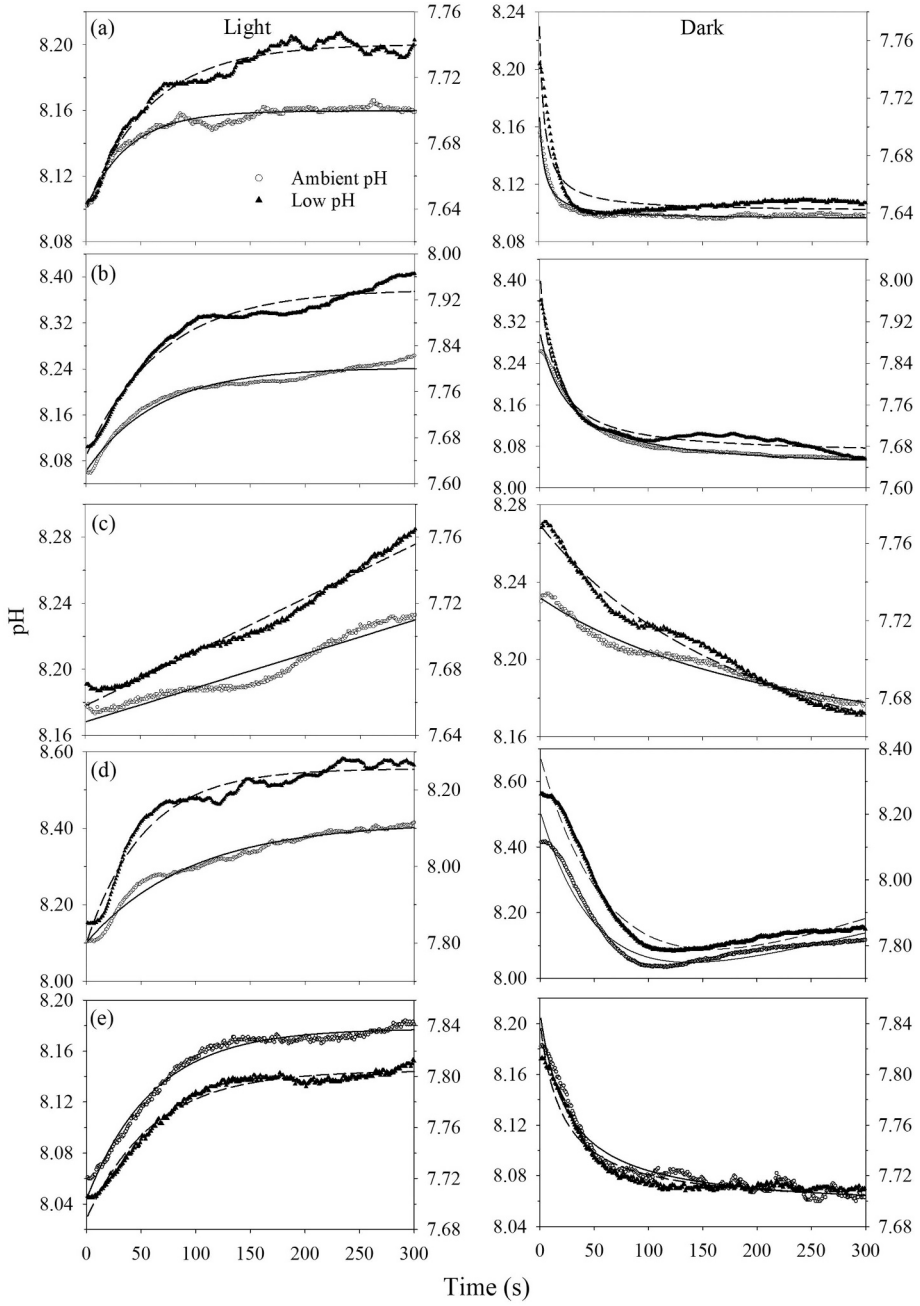

Fig. 4. pH light and dark thalli surface dynamics over the 300 s incubation under ambient and low pH for each species (a = *Neogoniolithon*, b = *Jania*, c = CCA, d = *Halimeda*, e = *Udotea*). The pH response in the light for all species fit an exponential rise to a maximum single 3-parameter model with the exception of CCA that fit a linear model. In the dark, pH decline over time was fit to a 3-parameter hyperbolic decay model with the exception of *Halimeda* that had an exponential decay function with a linear combination. Models, parameters and fits are presented in Table 4. Each point is the mean of 3 sequential runs (Fig. 2).

cell invaginations increasing their surface area to support H^+ pumping (Pueschel et al., 2005).

Although *Udotea*, CCA, and *Jania* did not demonstrate species-specific light/dark H^+ dynamics independent of PSII, they exhibited unique H^+ dynamics relative to the other species. *Udotea* was the only species that maintained higher thallus surface pH compared to bulk seawater, but no clear increase of pH under OA conditions relative to controls. This may have been due to diffusion limitation of CO_2 through filament sheaths, or a greater dependency on HCO_3^- even at low pH. This species has the most enriched C isotope ratio ($\delta^{13}C = -14‰$) amongst the five species, and lowered P_{gmax} by 40% when active (ATPase) ion transport was inhibited (Zweng et al., 2018), perhaps explaining why it was able to raise pH at the DBL in the light, but did not respond to greater DIC availability. CCA had a slower 2-phase increase in pH at the thalli surface in response to light. The shift in pH change with a steeper slope was coincident with a short-term stabilization or decline in surface O_2 concentration, followed by a rapid increase in O_2 flux. This response may be reflective of an initial active HCO_3^- uptake mechanism, followed by rapid CA_{ext}-driven DIC uptake. *Jania* responded similarly to irradiance, with a rapid 2-phase pH change corresponding to O_2 flux and an O_2 decrease or plateau between phases. While the 2-phase O_2/H^+ dynamics exhibit a similar pattern at 8.1 and 7.65 pH, the efficiency of pH change to O_2 flux was greater at low pH, consistent with a more rapid conversion of HCO_3^- to CO_2 by CA_{ext} due to a shift in the DIC chemical equilibria.

The combination of similar O_2 dynamics at 8.1 and 7.65 pH, despite

Table 4
Linear and non-linear regression models, fit (R^2) and parameters of the pH dynamics in the light and dark at the thalli surface (Neo = *Neogoniolithon*, Jan = *Jania*, CCA, Hal = *Halimeda*, Udot = *Udotea*) for 300 s dark-light cycles under ambient (A) and low (L) pH treatments. Data corresponds to models shown in Fig. 4.

Sp	pH	Equation	R^2	y0	a	b	c
Light							
Neo	A	y = y0 + a*(1−exp(−b*x))	0.95	8.1	0.059	0.0258	na
Neo	L	y = y0 + a*(1−exp(−b*x))	0.97	7.64	0.101	0.017	na
Jan	A	y = y0 + a*(1−exp(−b*x))	0.96	8.06	0.18	0.0156	na
Jan	L	y = y0 + a*(1−exp(−b*x))	0.96	7.65	0.29	0.0145	na
CCA	A	f = y0 + a*x	0.93	8.17	0.0002	na	na
CCA	A	f = y0 + a*x	0.98	7.65	0.0003	na	na
Hal	A	y = y0 + a*(1−exp(−b*x))	0.98	8.1	0.314	0.0105	na
Hal	L	y = y0 + a*(1−exp(−b*x))	0.96	7.8	0.455	0.0189	na
Udot	A	y = y0 + a*(1−exp(−b*x))	0.98	8.04	0.134	0.0165	na
Udot	L	y = y0 + a*(1−exp(−b*x))	0.98	7.69	0.116	0.0165	na
Dark							
Neo	A	y = y0 + (a*b)/(b + x)	0.93	8.1	0.091	3.53	na
Neo	L	y = y0 + (a*b)/(b + x)	0.82	7.64	0.167	3.38	na
Jan	A	y = y0 + (a*b)/(b + x)	0.99	8.03	0.272	24.45	na
Jan	L	y = y0 + (a*b)/(b + x)	0.95	7.66	0.362	11.69	na
CCA	A	y = y0 + (a*b)/(b + x)	0.97	8.13	0.102	266	na
CCA	A	y = y0 + (a*b)/(b + x)	0.98	7.59	0.179	248	na
Hal	A	y = y0 + a*exp.(−b*x) + c*x	0.96	7.9	0.615	0.02	0.0008
Hal	L	y = y0 + a*exp.(−b*x) + c*x	0.97	7.54	0.837	0.016	0.0011
Udot	A	y = y0 + (a*b)/(b + x)	0.96	8.05	0.158	25.06	na
Udot	L	y = y0 + (a*b)/(b + x)	0.95	7.69	0.148	20.66	na

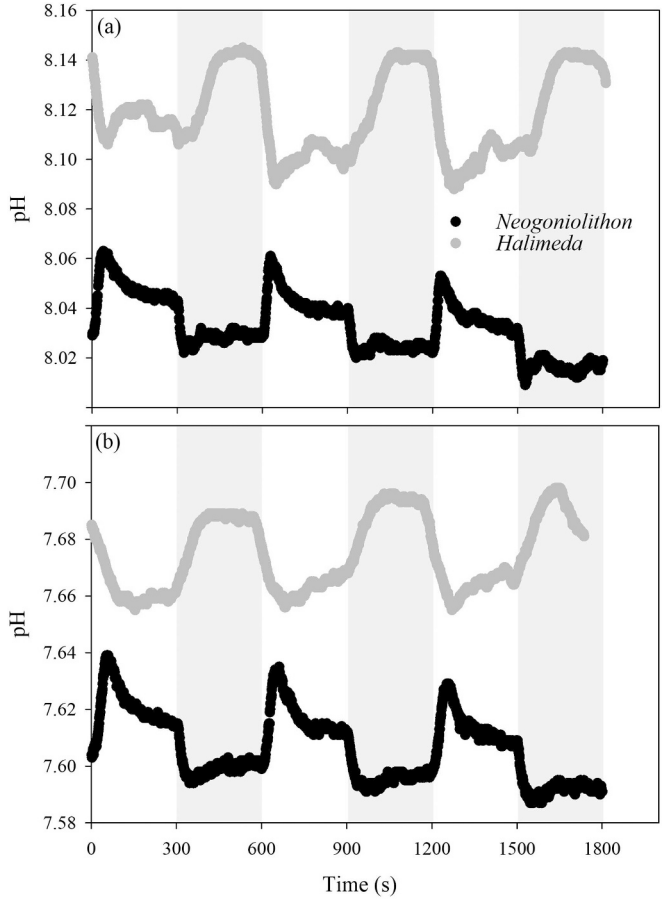

Fig. 5. Dynamics of light/dark pH cycles run at (a) ambient and (b) low pH in the presense of the photosystem II inhibitor DCMU. All runs were initiated in the light (300 s) followed by dark (300 s) periods. Three sequential replicated light/dark cycles are shown for *Neogoniolithon* and *Halimeda*.

a 3-fold increase in [CO_2] in the latter, $\delta^{13}C$ isotopic ratios of the species examined, rates of DBL pH change upon illumination at the thalli surface, and DIC modeling imply the use of CCMs that simultaneously support photosynthesis and calcification (Fig. 6). The CCMs are most likely comprised of a HCO_3^- uptake mechanism with a H^+ symport and/or OH^- antiport, or other Na^+/Ca^{2+} transport systems (Gimmler, 2000; Raven and Hurd, 2012; Taylor et al., 2012). CA_{ext} that enhances diffusive uptake of CO_2 (20–65%; Zweng et al., 2018), presumably in combination with proton pumps, may also be important (Fig. 6a). Based on our microsensor study, and applying equilibrium assumptions (CO2SYS), under ambient pH (~8.25, 5.8 nM H^+) in the light (Fig. 6a), HCO_3^- and CO_2 provide DIC for photosynthesis and all DIC species (~1494:323:6 μmol kg^{-1} HCO_3^-:CO_3^{2-}:CO_2) are available for calcification through diffusive and/or paracellular pathways. Photosynthesis also contributes ATP directly and via oxidative phosphorylation of photosynthates for energy-dependent ion transport and organic substrates important for crystal nucleation, lowering activation energy, and serving as catalysts, such as acid-rich proteins (Bilan and Usov, 2001; Borowitzka, 1982; Von Euw et al., 2017). Cellular CO_2 dehydrogenated by CA_{ext} is taken up by diffusion and immediately sequestered for photosynthesis or, because of its "leakiness" out of the cell for a CCM (Raven and Beardall, 2016), cellular CO_2 is hydrogenated by CA_{int} to HCO_3^- and H^+ (Fig. 6a). As part of this reaction, OH^- is available to neutralize H^+ in the cell wall or DBL. HCO_3^- is transported to the chloroplast for photosynthesis (or potentially used for calcification) and H^+ is sequestered by the cell or removed to maintain acid-base regulation. HCO_3^- uptake may also be driven by other symports/antiports (e.g., Na^+/Cl^-) and H^+/OH^- fluxes regulate acid/base conditions within the cells. The morphology of different macroalgal species provide variations on the role of diffusive versus active ion transport options into and out of the calcification site. For example, *Halimeda* species possess diffusive pathways to DIC, but appear to have a H^+ pump to expel protons out of the inter-cellular calcification site. Ion transport through cell walls or mucilage sheaths (e.g., *Udotea*) are primarily constrained by diffusion gradients, DBL microchemistry, potentially cell wall constituents, and/or are driven by ion transport across the plasmalemma. One rhodophyta species (*Neogoniolithon*), and another less

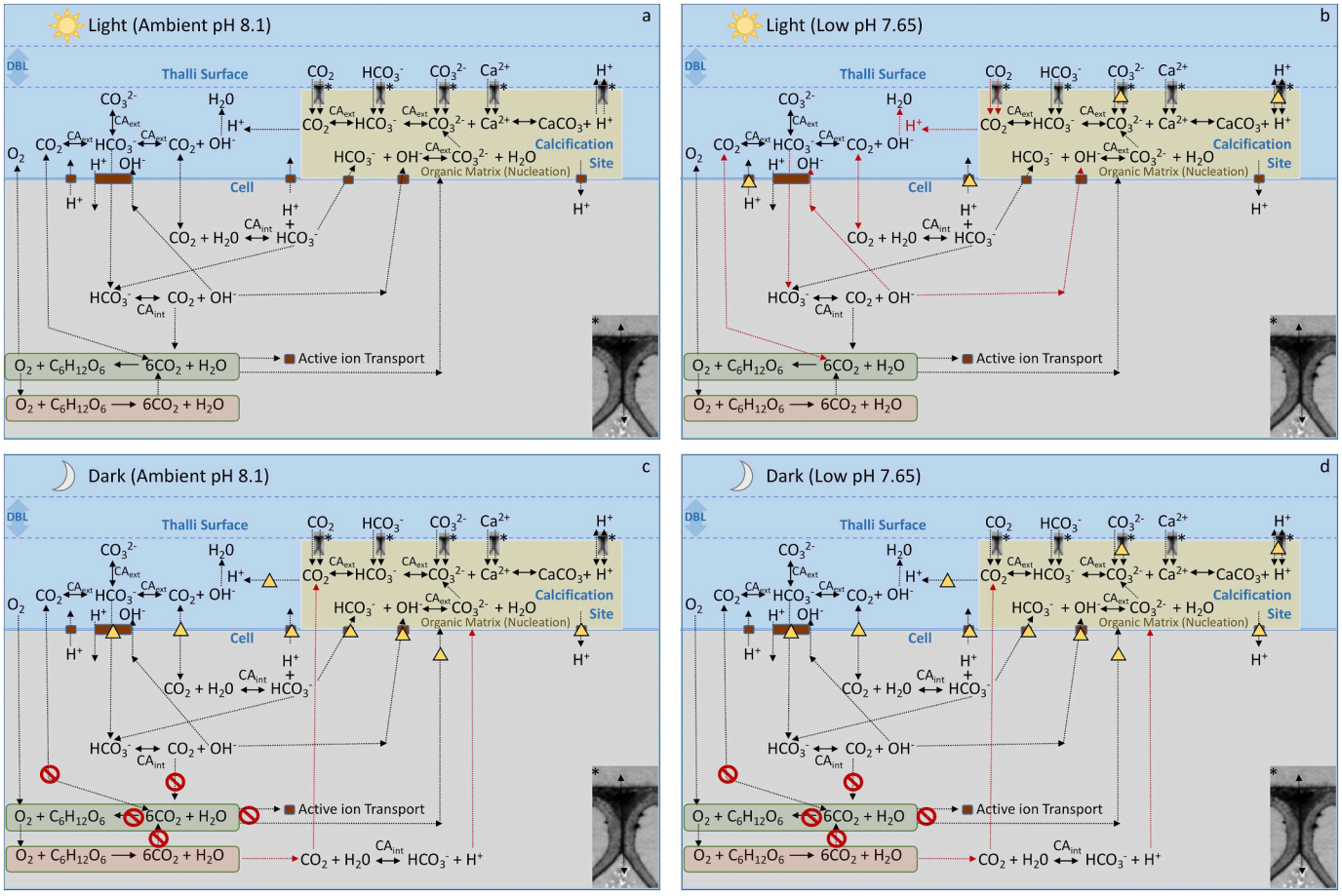

Fig. 6. Proposed model of DIC pathways and ion transport in the (a) light and (b) dark at ambient pH and (c) light and (d) dark at low pH indicative of ocean acidification (OA) for the year 2100, and the potential consequences for calcification (see text for details) in tropical marine macroalgae. Diffusive pathways between appressed surface filaments (utricles) are shown for *Halimeda*. Red dashed arrows depict potential changes in response to OA. The no symbol (∅) represent pathways that are limited and/or shut down under each scenario compared to the ambient pH conditions in the light (a). Yellow triangles (Δ) are proposed mechanisms or transport pathways that are predicted to slow or be negatively affected in the scenario relative to ambient pH conditions in the light (a). (For interpretation of the references to colour in this figure legend, the reader is referred to the web version of this article.)

consistently (*Jania*), showed evidence that they possess a PSII-independent light triggered proton pump supported by positive net calcification in the dark and in the light with DCMU (McNicholl and Koch, unpublished data).

Based on the present study, under low pH in the light (Fig. 6b), photosynthesis continues to sustain a high pH at the thalli surface even though [H^+] increases on average ~130% in the DBL (13.3 nM H^+) when pH increases from 7.65 to 7.91. As the carbonate equilibria shifts (~1822:192:17 μmol kg^{-1} HCO_3^-:CO_3^{2-}:CO_2) and CO_2 is taken up for photosynthesis, H^+ are neutralized by OH^- which can raise the DBL pH (Fig. 6b). Higher DBL [H^+] could also constrain cellular H^+ efflux involved in acid-base regulation, or as part of a HCO_3^- uptake mechanism, due to a lower concentration gradient at the plasmalemma reversing the proton motive force (Fig. 6b). Further, upregulation of a HCO_3^-/OH^- antiport cannot be ruled out (Fig. 6b). Therefore, CO_2 uptake by diffusion, H^+ sequestration through HCO_3^- dehydration and CO_2 uptake, and/or OH^- efflux to the DBL are all photosynthesis-driven mechanisms that could raise the DBL pH and Ω_{CaCO3} at macroalgal calcification sites under OA in the light (Fig. 6b). These results support observations of sustained calcification in the light by these species under OA even though equilibria chemistry (CO2SYS) predicts a 47% decrease in DBL [CO_3^{2-}] based on averages in this study.

In the dark, H^+ are not efficiently removed from the DBL and calcifying space even at ambient pH (Fig. 6c). Compounding this potential acidification problem is an internal accumulation of respiratory CO_2 that would need to diffuse out of the cell, or be hydrolyzed to HCO_3^- and H^+. Subsequently, the H^+ would need to be exported across the plasma membrane for acid-base regulation, and the respiratory CO_2 sequestered in $CaCO_3$. In addition to acid-base issues within and external to the cell, energetics from photosynthesis, and potentially organics for nucleation and other processes required to sustain optimal conditions for calcification are reduced. Although we measured modest increases in pH at the thalli surface relative to bulk seawater in the dark, only two rhodophyte species (*Neogoniolithon*, *Jania*) were able to maintain net positive calcification in the dark at ambient pH (McNicholl and Koch, unpublished data). Under OA in the dark, all species examined herein (McNicholl and Koch, unpublished data) and by Kamenos et al. (2013) (*Lithothamnion glaciale*) exhibited net dissolution at average pH of 7.72 (19.4 nM H^+) when CO_3^{2-} levels declined (~1984:128:26 μmol kg^{-1} HCO_3^-:CO_3^{2-}:CO_2).

Thus, for marine calcifying macroalgae, photosynthesis is critical to remove H^+ from the DBL, promote ion flux that supports CCMs and DBL chemistry, and cellular acid-base homeostasis, particularly under OA conditions. While some rhodophytes sustain H^+ pumps and calcification in the dark, at low pH in the dark, ion pumps likely become overwhelmed by high DBL CO_2 and H^+, even though they maintain the DBL pH above the bulk seawater. Certainly, additional studies are required to further identify tropical macroalgae species-specific

mechanisms of DIC uptake for photosynthesis and how these are linked to ion transport mechanisms that impact calcification. Also, there is great interest in how increases in seawater [H^+] and DIC speciation with ongoing OA will influence these mechanisms on short and long time scales that incorporate acclimation and adaptation.

Declaration of Competing Interest

None.

Acknowledgements

We recognize the following graduate and undergraduate students (Regina Zweng, Chris Johnson, Dr. Kate Peach, Kim McFarlane) for field assistance and staff at Unisense for microsensor training and troubleshooting. Two anonymous reviews significantly improved this manuscript. Discussions with Drs. John Raven, Kim Yates, Mary Bison and George Bowes assisted in our interpretation of the data and proposed mechanisms; Dr. Raven is especially recognized for kindly reviewing the manuscript and providing constructive comments based on his expansive knowledge of macroalgal physiology. This research was funded by the National Science Foundation, United States through Grant #140-381.

Appendix A. Supplementary data

Supplementary data to this article can be found online at https://doi.org/10.1016/j.jembe.2019.151208.

References

Anthony, K.R.N., Kline, D.I., Diaz-Pulido, G., Dove, S., Hoegh-Guldberg, O., 2008. Ocean acidification causes bleaching and productivity loss in coral reef builders. Proc. Natl. Acad. Sci. 105, 17442–17446. https://doi.org/10.1073/pnas.0804478105.

Bach, L.T., 2015. Reconsidering the role of carbonate ion concentration in calcification by marine organisms. Biogeosci. Discuss. 12, 6689–6722. https://doi.org/10.5194/bg-12-6689-2015.

Bilan, M.I., Usov, A.I., 2001. Polysaccharides of calcareous algae and their effect on the calcification process. Russ. J. Bioorganic Chem. 27, 4–20.

Borowitzka, M.A., 1981. Photosynthesis and calcification in the articulated coralline red algae *Amphiroa anceps* and *A. foliacea*. Mar. Biol. 62, 17–23. https://doi.org/10.1007/BF00396947.

Borowitzka, M.A., 1982. Morphological and cytological aspects of algal calcification. Int. Rev. Cytol. 74, 127–162. https://doi.org/10.1016/S0074-7696(08)61171-7.

Borowitzka, M.A., Larkum, A.W.D., 1987. Calcification in algae: mechanisms and the role of metabolism. CRC. Crit. Rev. Plant Sci. 6, 1–45. https://doi.org/10.1080/07352688709382246.

Caldeira, K., Wickett, M.E., 2003. Oceanography: anthropogenic carbon and ocean pH. Nature 425, 365. https://doi.org/10.1038/425365a.

Chrachri, A., Hopkinson, B.M., Flynn, K., Brownlee, C., Wheeler, G.L., 2018. Dynamic changes in carbonate chemistry in the microenvironment around single marine phytoplankton cells. Nat. Commun. 1–12. https://doi.org/10.1038/s41467-017-02426-y.

Comeau, S., Carpenter, R.C., Edmunds, P.J., 2012. Coral reef calcifiers buffer their response to ocean acidification using both bicarbonate and carbonate. Proc. R. Soc. B 280, 1–8. https://doi.org/10.1098/rspb.2012.2374.

Comeau, S., Carpenter, R., Edmunds, P., 2016. The effects of pCO_2 on photosynthesis and respiration of tropical scleractinian corals and calcified algae. ICES J. Mar. Sci. https://doi.org/10.1093/icesjms/fsv267.

Comeau, S., Cornwall, C.E., DeCarlo, T.M., Krieger, E., McCulloch, M.T., 2018. Similar controls on calcification under ocean acidification across unrelated coral reef taxa. Glob. Chang. Biol. 24, 1–12. https://doi.org/10.1111/gcb.14379.

Cornwall, C.E., Hepburn, C.D., Pritchard, D., Currie, K.I., Mcgraw, C.M., Hunter, K.A., Hurd, C.L., 2012. Carbon-use strategies in macroalgae: differential responses to lowered pH and implications for ocean acidification. J. Phycol. 48, 137–144. https://doi.org/10.1111/j.1529-8817.2011.01085.x.

Cornwall, C.E., Hepburn, C.D., Pilditch, C.A., Hurd, C.L., 2013. Concentration boundary layers around complex assemblages of macroalgae: implications for the effects of ocean acidification on understory coralline algae. Limnol. Oceanogr. 58, 121–130. https://doi.org/10.4319/lo.2013.58.1.0121.

Cornwall, C.E., Boyd, P.W., McGraw, C.M., Hepburn, C.D., Pilditch, C.A., Morris, J.N., Smith, A.M., Hurd, C.L., 2014. Diffusion boundary layers ameliorate the negative effects of ocean acidification on the temperate coralline macroalga *Arthrocardia corymbosa*. PLoS One 9, 1–9. https://doi.org/10.1371/journal.pone.0097235.

Cornwall, C.E., Pilditch, C.A., Hepburn, C.D., Hurd, C.L., 2015. Canopy macroalgae influence understorey corallines' metabolic control of near-surface pH and oxygen concentration. Mar. Ecol. Prog. Ser. 525, 81–95. https://doi.org/10.3354/meps11190.

Cornwall, C.E., Comeau, S., McCulloch, M.T., 2017a. Coralline algae elevate pH at the site of calcification under ocean acidification. Glob. Chang. Biol. 23, 4245–4256. https://doi.org/10.1111/gcb.13673.

Cornwall, C.E., Revill, A.T., Hall-Spencer, J.M., Milazzo, M., Raven, J.A., Hurd, C.L., 2017b. Inorganic carbon physiology underpins macroalgal responses to elevated CO_2. Sci. Rep. 7, 1–12. https://doi.org/10.1038/srep46297.

Cyronak, T., Schulz, K.G., Jokiel, P.L., 2015. The Omega myth: what really drives lower calcification rates in an acidifying ocean. ICES J. Marine Sci. 1–5. https://doi.org/10.1093/icesjms/fsv075.

De Beer, D., Larkum, A.W.D., 2001. Photosynthesis and calcification in the calcifying algae *Halimeda discoidea* studied with microsensors. Plant Cell Environ. 24, 1209–1217. https://doi.org/10.1046/j.1365-3040.2001.00772.x.

Donald, H.K., Ries, J.B., Stewart, J.A., Fowell, S.E., Foster, G.L., 2017. Boron isotope sensitivity to seawater pH change in a species of *Neogoniolithon* coralline red alga. Geochim. Cosmochim. Acta 217, 240–253. https://doi.org/10.1016/j.gca.2017.08.021.

Doney, S.C., Fabry, V.J., Feely, R.A., Kleypas, J.A., 2009. Ocean acidification: the other CO_2 problem. Annu. Rev. Mar. Sci. 1, 169–192. https://doi.org/10.1146/annurev.marine.010908.163834.

Doney, S.C., Ruckelshaus, M., Duffy, J.E., Barry, J.P., Chan, F., English, C.A., Galindo, H.M., Grebmeier, J.M., Hollowed, A.B., Knowlton, N., Polovina, J., Rabalais, N.N., Sydeman, W.J., Talley, L.D., 2012. Climate change impacts on marine ecosystems. Annu. Rev. Mar. Sci. 4, 11–37. https://doi.org/10.1146/annurev-marine-041911-111611.

Dutra, E., Koch, M., Peach, K.E., Manfrino, C., 2015. Tropical crustose coralline algal individual and community responses to elevated pCO_2 under high and low irradiance. ICES J. Mar. Sci. 707–721.

Fabry, V.J., Seibel, B., Feely, R., Orr, J., 2008. Impacts of ocean acidification on marine fauna and ecosystem processes. Int. Counc. Explor. Sea 414–432. https://doi.org/10.1093/icesjms/fsn048.

Gao, K., Aruga, Y., Asada, K., Ishihara, T., Akano, T., Kiyohara, M., 1993. Calcification in the articulated coralline alga *Corallina pilulifera*, with special reference to the effect of elevated CO_2 concentration. Mar. Biol. 117, 129–132. https://doi.org/10.1007/BF00346434.

Gattuso, J.-P., Allemand, D., Frankignoulle, M., 1999. Photosynthesis and calcification at cellular, organismal and community levels in coral reefs: a review on interactions and control by carbonate chemistry. Am. Zool. 39, 160–183. https://doi.org/10.1093/icb/39.1.160.

Gattuso, J.-P., Magnan, A., Bille, R., Cheung, W.W.L., Howes, E.L., Joos, F., Allemand, D., Bopp, L., Cooley, S.R., Eakin, C.M., Hoegh-Guldberg, O., Kelly, R.P., Portner, H.-O., Rogers, A.D., Baxter, J.M., Laffoley, D., Osborn, D., Rankovic, A., Rochette, J., Sumaila, U.R., Treyer, S., Turley, C., 2015. Contrasting futures for ocean and society from different anthropogenic CO_2 emissions scenarios. Science (80-.) 349, aac4722-1–aac4722-10. https://doi.org/10.1126/science.aac4722.

Gehlen, M., Séférian, R., Jones, D.O.B., Roy, T., Roth, R., Barry, J., Bopp, L., Doney, S.C., Dunne, J.P., Heinze, C., Joos, F., Orr, J.C., Resplandy, L., Segschneider, J., Tjiputra, J., 2014. Projected pH reductions by 2100 might put deep North Atlantic biodiversity at risk. Biogeosciences 11, 6955–6967. https://doi.org/10.5194/bg-11-6955-2014.

Gimmler, H., 2000. Primary sodium plasma membrane ATPases in salt-tolerant algae: facts and fictions. J. Exp. Bot. 51, 1171–1178. https://doi.org/10.1093/jxb/51.348.1171.

Hartin, C.A., Bond-Lamberty, B., Patel, P., Mundra, A., 2016. Ocean acidification over the next three centuries using a simple global climate carbon-cycle model: projections and sensitivities. Biogeosciences 13, 4329–4342. https://doi.org/10.5194/bg-13-4329-2016.

Hendriks, I.E., Duarte, C.M., Álvarez, M., 2010. Vulnerability of marine biodiversity to ocean acidification: a meta-analysis. Estuar. Coast. Shelf Sci. 86, 157–164. https://doi.org/10.1016/j.ecss.2009.11.022.

Hoegh-Guldberg, O., Mumby, P.J., Hooten, A.J., Steneck, R.S., Greenfield, P., Gomez, E., Harvell, C.D., Sale, P.F., Edwards, A.J., Caldeira, K., Knowlton, N., Eakin, C.M., Iglesiaia-Prieto, R., Muthiga, N., Bradbury, R.H., Dubi, A., Hatziolos, M.E., 2007. Coral reefs under rapid climate change and ocean acidification. Science (80-.) 318, 1737–1742. https://doi.org/10.1126/science.1152509.

Hofmann, L.C., Koch, M., De Beer, D., 2016. Biotic control of surface pH and evidence of light-induced H^+ pumping and Ca^{2+}-H^+ exchange in a tropical crustose coralline alga. PLoS One 11, 1–24. https://doi.org/10.1371/journal.pone.0159057.

Hofmann, L.C., Schoenrock, K., de Beer, D., 2018. Arctic coralline algae elevate surface pH and carbonate in the dark. Front. Plant Sci. 9, 1–12. https://doi.org/10.3389/fpls.2018.01416.

Hurd, C.L., Cornwall, C.E., Currie, K., Hepburn, C.D., McGraw, C.M., Hunter, K.A., Boyd, P.W., 2011. Metabolically induced pH fluctuations by some coastal calcifiers exceed projected 22nd century ocean acidification: a mechanism for differential susceptibility? Glob. Chang. Biol. 17, 3254–3262. https://doi.org/10.1111/j.1365-2486.2011.02473.x.

IPCC, 2013. Climate Change 2013: The Physical Science Basis. Contribution of Working Group I to the Fifth Assessment Report of the Intergovernmental Panel on Climate Change. Cambridge University Press, Cambridge, United Kingdom and New York, NY, USA. https://doi.org/10.1017/CBO9781107415324.

Johnston, A.A.M., Maberly, S.C., Raven, J.A., 1992. The Acquisition of Inorganic Carbon by Four Red Macroalgae 92. pp. 317–326 (https://doi.org/http://www.jstor.org/stable/4220171).

Jokiel, P.L., 2011. Ocean acidification and control of reef coral calcification by boundary layer limitation of proton flux. Bull. Mar. Sci. 87, 639–657. https://doi.org/10.5343/bms.2010.1107.

Jokiel, P.L., 2013. Coral reef calcification: carbonate, bicarbonate and proton flux under conditions of increasing ocean acidification. Proc. R. Soc. B Biol. Sci. 280, 1–4. https://doi.org/10.1098/rspb.2013.0031.

Kamenos, N.A., Burdett, H.L., Aloisio, E., Findlay, H.S., Martin, S., Longbone, C., Dunn, J., Widdicombe, S., Calosi, P., 2013. Coralline algal structure is more sensitive to rate, rather than the magnitude, of ocean acidification. Glob. Chang. Biol. 19, 3621–3628. https://doi.org/10.1111/gcb.12351.

Koch, M., Bowes, G., Ross, C., Zhang, X.-H., 2013. Climate change and ocean acidification effects on seagrasses and marine macroalgae. Glob. Chang. Biol. 19. https://doi.org/10.1111/j.1365-2486.2012.02791.x.

Kroeker, K., Kordas, R., Singh, G., 2010. Meta-analysis reveals negative yet variable effects of ocean acidification on marine organisms. Ecol. Lett. 13, 1419–1434. https://doi.org/10.1111/j.1461-0248.2010.01518.x.

Langdon, C., Takahashi, T., Sweeney, C., Chipman, D., Goddard, J., Marubini, F., Aceves, H., Barnett, H., Atkinson, M.J., 2000. Effect of calcium carbonate saturation state on the calcification rate of an experimental coral reef. Glob. Biogeochem. Cycles 14, 639–654.

Maberly, A.S.C., Raven, J.A., Johnston, A.M., 1992. Discrimination between ^{12}C and ^{13}C by marine plants. Oecologia 91, 481–492.

Martin, S., Charnoz, A., Gattuso, J.P., 2013. Photosynthesis, respiration and calcification in the Mediterranean crustose coralline alga *Lithophyllum cabiochae* (Corallinales, Rhodophyta). Eur. J. Phycol. 48, 163–172. https://doi.org/10.1080/09670262.2013.786790.

McCulloch, M., Trotter, J., Montagna, P., Falter, J., Dunbar, R., Freiwald, A., Försterra, G., López Correa, M., Maier, C., Rüggeberg, A., Taviani, M., 2012. Resilience of cold-water scleractinian corals to ocean acidification: boron isotopic systematics of pH and saturation state up-regulation. Geochim. Cosmochim. Acta 87, 21–34. https://doi.org/10.1016/j.gca.2012.03.027.

McDonald, M.R., McClintock, J.B., Amsler, C.D., Rittschof, D., Angus, R.A., Orihuela, B., Lutostanski, K., 2009. Effects of ocean acidification over the life history of the barnacle *Amphibalanus amphitrite*. Mar. Ecol. Prog. Ser. 385, 179–187. https://doi.org/10.3354/meps08099.

Millero, F.J., 2007. The marine inorganic carbon cycle. Chem. Rev. 107, 308–341. https://doi.org/10.1021/cr0503557.

Millero, F.J., Graham, T.B., Huang, F., Bustos-Serrano, H., Pierrot, D., 2006. Dissociation constants of carbonic acid in seawater as a function of salinity and temperature. Mar. Chem. 100, 80–94. https://doi.org/10.1016/j.marchem.2005.12.001.

Noisette, F., Hurd, C., 2018. Abiotic and biotic interactions in the diffusive boundary layer of kelp blades create a potential refuge from ocean acidification. Funct. Ecol. 32, 1329–1342. https://doi.org/10.1111/1365-2435.13067.

Orr, J.C., Fabry, V.J., Aumont, O., Bopp, L., Doney, S.C., Feely, R.A., Gnanadesikan, A., Gruber, N., Ishida, A., Joos, F., Key, R.M., Lindsay, K., Maier-Reimer, E., Matear, R., Monfray, P., Mouchet, A., Najjar, R.G., Plattner, G.-K., Rodgers, K.B., Sabine, C.L., Sarmiento, J.L., Schlitzer, R., Slater, R.D., Totterdell, I.J., Weirig, M.-F., Yamanaka, Y., Yool, A., 2005. Anthropogenic ocean acidification over the twenty-first century and its impact on calcifying organisms. Nature 437, 681–686. https://doi.org/10.1038/nature04095.

Peach, K.E., Koch, M.S., Blackwelder, P.L., Guerrero-Given, D., Kamasawa, N., 2017a. Primary utricle structure of six *Halimeda* species and potential relevance for ocean acidification tolerance. Bot. Mar. 60, 1–11. https://doi.org/10.1515/bot-2016-0055.

Peach, K.E., Koch, M.S., Blackwelder, P.L., Manfrino, C., 2017b. Calcification and photophysiology responses to elevated pCO_2 in six *Halimeda* species from contrasting irradiance environments on Little Cayman Island reefs. J. Exp. Mar. Bio. Ecol. 486, 114–126. https://doi.org/10.1016/j.jembe.2016.09.008.

Pierrot, D., Lewis, E., Wallace, D., 2006. MS Excel Program Developed for CO_2 Systems Calculations: ORNL/CDIAC 105a.

Pueschel, C.M., Judson, B.L., Wegeberg, S., 2005. Decalcification during epithallial cell turnover in Jania adhaerens (Corallinales, Rhodophyta). Phycologia 44, 156–162. https://doi.org/10.2216/0031-8884(2005)44[156:DDECTI]2.0.CO;2.

Raven, J.A., Beardall, J., 2016. The ins and outs of CO_2. J. Exp. Bot. 67, 1–13. https://doi.org/10.1093/jxb/erv451.

Raven, J.A., Hurd, C.L., 2012. Ecophysiology of photosynthesis in macroalgae. Photosynth. Res. 113, 105–125. https://doi.org/10.1007/s11120-012-9768-z.

Riahi, K., Rao, S., Krey, V., Cho, C., Chirkov, V., Fischer, G., Kindermann, G., Nakicenovic, N., Rafaj, P., 2011. RCP 8.5-A scenario of comparatively high greenhouse gas emissions. Clim. Chang. 109, 33–57. https://doi.org/10.1007/s10584-011-0149-y.

Riebesell, U., Gattuso, J., 2011. Guide to Best Practices for Ocean Acidification Research and Data Reporting. https://doi.org/10.2777/66906.

Rodolfo-Metalpa, R., Houlbrèque, F., Tambutté, É., Boisson, F., Baggini, C., Patti, F.P., Jeffree, R., Fine, M., Foggo, A., Gattuso, J.P., Hall-Spencer, J.M., 2011. Coral and mollusc resistance to ocean acidification adversely affected by warming. Nat. Clim. Chang. 1–5. https://doi.org/10.1038/nclimate1200.

Sabine, C.L., Feely, R.A., Gruber, N., Key, R.M., Lee, K., Bullister, J.L., Wanninkhof, R., Wong, C.S., Wallace, D.W.R., Tilbrook, B., Millero, F.J., Peng, T.-H., Kozyr, A., Ono, T., Rios, A.F., 2004. The oceanic sink for anthropogenic CO_2. Science 305, 367–371. https://doi.org/10.1126/science.1097403.

Shamberger, K.E.F., Cohen, A.L., Golbuu, Y., McCorkle, D.C., Lentz, S.J., Barkley, H.C., 2014. Diverse coral communities in naturally acidified waters of a western Pacific reef. Geophys. Res. Lett. 1–6. https://doi.org/10.1002/2013GL058489.

Taylor, A.R., Brownlee, C., Wheeler, G.L., 2012. Proton channels in algae: reasons to be excited. Trends Plant Sci. 17, 675–684. https://doi.org/10.1016/j.tplants.2012.06.009.

Von Euw, S., Zhang, Q., Manichev, V., Murali, N., Gross, J., Feldman, L.C., Gustafsson, T., Flach, C., Mendelsohn, R., Falkowski, P.G., 2017. Biological control of aragonite formation in stony corals. Science (80-.). 356, 933–938. https://doi.org/10.1126/science.aam6371.

Waldbusser, G.G., Hales, B., Haley, B.A., 2016. Comment: calcium carbonate saturation state: on myths and this or that stories. ICES J. Mar. Sci. 73, 563–568. https://doi.org/10.1093/icesjms/fsv174.

Wizemann, A., Meyer, F.W., Westphal, H., 2014. A new model for the calcification of the green macro-alga *Halimeda opuntia* (Lamouroux). Coral Reefs 1–14. https://doi.org/10.1007/s00338-014-1183-9.

Zweng, R.C., Koch, M.S., Bowes, G., 2018. The role of irradiance and C-use strategies in tropical macroalgae photosynthetic response to ocean acidification. Sci. Rep. 8, 1–11. https://doi.org/10.1038/s41598-018-27333-0.